Infrared observations of Io from Juno.

1

2 A. Mura, A. Adriani, F. Tosi, R. M. C. Lopes, G. Sindoni, G. Filacchione, D. A. Williams, A. G.

3 Davies, C. Plainaki, S. Bolton, F. Altieri, A. Cicchetti, D. Grassi, A. Migliorini, M.L. Moriconi,

4 R. Noschese, A. Olivieri, G. Piccioni, R. Sordini

5

6 **Abstract**. The Jovian InfraRed Auroral Mapper (JIRAM) on board the NASA Juno

7 spacecraft is a dual-band imager and spectrometer, primarily designed to study the

8 Jovian atmosphere and aurorae. In addition to its primary goal, JIRAM has been used to

9 obtain images and spectra of the Galilean satellites, Jupiter's largest moons, when the

10 spacecraft attitude was favourable to achieve this goal. Here we present JIRAM's first

11 images and spectra of Io. These observations are used to characterize the location and

12 possible morphology, and some temperatures, of Io's volcanic thermal sources; the

13 identification of SO_2 and the possible identification of other materials. A new hot

14 spot/volcano is identified close to the South Pole of Io, and others are seen in lower

15 latitude regions, which were previously unmapped. Images of the same region taken 2

16 months apart also show variations of hot spot intensity, possibly due to new lava flows

17 or to lava flow breakouts.

18

19 Key points:

20 Juno's JIRAM investigation reveals new volcanic hot spots

21 Identification of spectral signatures in the dayside-averaged I/F

22 Thermal characterization of Io's hot spots

23

1. Introduction

Jupiter's moon Io is the only extra-terrestrial body where active silicate volcanism has been confirmed, and it is the most volcanically active body in the Solar System, by any measure of power output, discharge rate, volume erupted and the areal extent of lava flows and lava lakes (Lopes et al., 2004; Lopes and Spencer, 2007; Davies, 2007). This extreme level of volcanism is the result of tidal heating, which is maintained by the Laplace orbital resonance between Io, Europa, and Ganymede (Peale et al., 1979). After the discovery of active volcanism by the Voyager spacecraft (Morabito et al., 1979), numerous hot spots, some unambiguously at silicate eruption temperatures, were detected both using ground-based telescopes (e.g. Veeder et al., 1994; Marchis et al., 2005; de Kleer and de Pater, 2016a,b; Cantrall et al., 2018) and several spacecrafts: Voyager in 1979 (see summaries in Spencer and Schneider, 1996; Davies, 2007; Lopes and Spencer, 2007), Galileo from 1996 through 2002, Cassini in 2000 and 2001 (summarized by Lopes and Williams, 2005, Davies, 2007), and the New Horizons flyby in 2007 (Spencer et al., 2007). A full inventory of volcanic thermal sources up to the end of the Galileo epoch identified 250 volcanic centres (Veeder et al., 2015) enabling the first global map of Io's volcanic heat flow to be made. Ground-based telescopes equipped with adaptive optics have mapped global thermal and temporal variability and have identified at least 14 more active volcanoes (de Kleer and de Pater, 2016a,b; de Pater et al., 2017; Cantrall et al., 2018). Io's total heat flow was determined from ground based observations to be $1.05 \pm 0.12 \times 10^{14}$ W or equivalently 2.52 W/m^2 (Veeder et al., 1994), of which 54% emanates from volcanic hot spots (Veeder et al., 2015). The distribution of the remaining heat flow is unknown, but averaged over Io is approximately 1 W/m^2.

Io's mantle composition is thought to be predominantly silicates, but its surface is dominated by sulfur compounds (Carlson et al. 2001, 2007). Sulfur dioxide is ubiquitous on Io's surface, and sulfur and sulfur dioxide have been detected in Io's plumes (Spencer et al., 2000;). Although derived maximum temperatures of active lavas on Io indicate that they are silicate in composition (mostly basaltic, but possibly some ultramafic compositions; Davies et al., 1997; 2001; McEwen et al. 1998), it is likely that secondary sulfur flows also exist (Williams et al. 2001). Among the remaining questions after the

55 completion of the previous Jupiter-orbiting mission, Galileo, are the composition of Io's
56 lavas (e.g., Keszthelyi et al., 2007; Davies, 2007); possible differences in styles of
57 volcanic activity between lower and higher latitudes, as well as longitudinally (e.g.,
58 Davies et al., 2015; de Kleer and de Pater, 2016a,b) linked to the location and magnitude
59 of tidal heating; the distribution and magnitude of Io's non-volcanic background heat
60 flow (Veeder et al., 2012, 2015; Hamilton et al., 2013; Davies et al., 2015); and what
61 species besides sulfur and SO_2 are present on the surface (e.g., Marchis et al., 2007).

62 The Jovian Infrared Auroral Mapper (JIRAM, Adriani et al., 2008, 2014, 2016) is an
63 imaging spectrometer on board the Juno spacecraft, which started observing Jupiter in
64 August 2016 (Bolton et al., 2017). The JIRAM investigation was purposely designed to
65 explore the Jovian aurorae and the planet's atmospheric structure, dynamics and
66 composition. Although observation of the Galilean moons is not among the prime
67 objectives of the experiment, JIRAM can take advantage of the frequent observation
68 opportunities of the moons (usually, once per orbit) to collect infrared images and
69 spectra of their surfaces. Similar opportunities were exploited by JIRAM to observe
70 Europa's surface (Filacchione et al., 2019). So far, Io has been observed by JIRAM during
71 orbits 7, 9, 10, 17, 18 with a maximum ground resolution of 68 km per pixel,
72 significantly better than nearly all the observations obtained from the Near-Infrared
73 Mapping Spectrometer on-board the NASA Galileo spacecraft prior to its close flybys of
74 Io (Lopes-Gautier et al., 1999). In the future, a couple of close encounters are further
75 foreseen, which will allow JIRAM to collect images and spectra achieving 50 km per
76 pixel resolution, or better. In view of these future observations we present here the data
77 acquired so far, which characterize the location and size of the hot spots of Io, the mean
78 I/F for different orbits and the temperature of selected locations on the surface of Io.

79 JIRAM's observations of Io are particularly valuable as they significantly increase our
80 spatial, spectral, and temporal coverage of Io's polar regions, while also acquiring data
81 from lower latitudes. Prior to Juno, close observations of Io were mostly obtained from
82 an essentially equatorial geometry, thus creating a bias in the available datasets.
83 Voyager, Galileo and New Horizon data obtained only partial and limited coverage of
84 Io's polar regions (e.g., Mazurka et al., 1979; Smith et al., 1979; Perry et al. 2007; Veeder
85 et al., 2012; Tsang et al., 2014; Davies et al., 2015; Rathbun et al., 2018).

86

87   JIRAM data allows the identification of hot spots at both mid and high latitudes, thus
88   allowing modification to be made of previous models of volcanic heat flow, and the
89   volcanic contribution to Io's global heat flow. In the work presented here, a new hot
90   spot/volcano is identified close to the South Pole of Io, and ~5 more are identified in a
91   previously unmapped region; the images also show significant variations of the hot spot
92   distribution and extent.

93   The increase in spectral resolution compared to Galileo NIMS data allows us to examine
94   surface composition in a way that could not be done from Galileo. Spectral observations
95   by NIMS were hampered by radiation damage to the instrument during the spacecraft's
96   Io flybys, resulting in a stuck grating and much reduced spectral resolution for
97   observations at resolutions higher than ~200 km/pixel (Lopes et al., 2001, Douté et al.,
98   2001).

2. Data set

100   JIRAM combines two optical channels (imager and spectrometer) in one instrument; the
101   optical design uses a modified Schmidt telescope joined to a dual spectral channel
102   camera and to a grating spectrometer in Littrow configuration. Two distinct focal plane
103   detectors are used for imaging and spectroscopy, and the aberrations in the telescope
104   and spectrograph optical path are corrected by means of dioptric doublets. The
105   instrument uses a dedicated de-spinning mirror to compensate for the spacecraft
106   rotation (~2 rpm). The instrument is designed to perform one acquisition, consisting of
107   two 2D images in L-M spectral ranges and a 1D slit with full spectral resolution, during
108   every spacecraft rotation. JIRAM can tilt its field of view (FoV) along the plane
109   perpendicular to the Juno spin axis by delaying or anticipating the acquisition, which by
110   default is taken when the boresight points toward the center of Jupiter. JIRAM cannot
111   articulate its FoV in any other direction without requiring a spacecraft re-orientation.

112   The imager channel is a single detector (266 x 432 pixels) with 2 different filters (128 x
113   432 px each), separated by a 10-pixel wide inactive strip. The pixel angular resolution
114   (IFOV) is 0.01°. Hence, the FoV of both the L and M bands is 5.87° by 1.74°. The
115   responsivity of both imager channels is 2×10^6 DN / (W m^{-2} sr^{-1} s^{-1}).

116   Of the two filters, one (L, bandpass from 3.3 to 3.6 μm) was designed to detect the H3+
117   emission from Jupiter, while the other (M, bandpass from 4.5 to 5 μm) is meant to map

the thermal structures of Jupiter's atmosphere. When looking at Io, the L band is more sensitive to reflected sunlight than the M band, which is more sensitive to thermal emission. Hence, the L band is seldom used, also because if the target is completely in the L frame, then the spectrometer slit would receive no signal. An example of a L-band filter image of Io is shown in Figure 1. The M-band filter and the spectrometer have been extensively used to image the thermal emission from Io and more than 500 images and spectra have been collected so far.

The spectrometer channel is able to simultaneously acquire 336 spectral samples per pixel with 256 spatial pixels along the slit, and is placed inside the *M*-band filter FoV. Each spectrum covers the spectral range 2–5 μm, with an average spectral sampling of 9 nm/band. The noise equivalent spectral radiance (NESR) has a mean value of 10^{-4} W/(m^2 sr μm). The spectrometer cannot acquire contiguous slits on Io's surface due to the combination of the high orbital speed of Juno, low repetition rate (1 slit acquisition per spacecraft rotation) and on-board software temporal resolution. As a result, the projections of the spectrometer's slit are placed at different positions across Io's surface, with a pointing strategy that aims to distribute them uniformly. When necessary, JIRAM data is mapped onto the surface of Io using SPICE/NAIF routines and ancillary data (Acton, 1996). Table 1 contains a summary of the observations used in this study.

3. Infrared images and spectral analysis

Figure 2 shows the dayside I/F spectra as observed in different orbits: orbit 7 (Jul. 10th 2017, blue line), orbit 9 (Oct. 24th, 2017, red line) and 10 (Dec. 17th 2017, yellow line). Io's daytime 2-5 μm spectra as observed by JIRAM are dominated by solar reflection up to about 4 μm, while far away from hot spot locations the thermal emission on the dayside is typically revealed at wavelengths longer than 4 μm. The magenta line is the average spectrum.

Infrared spectra of Io in the 2-5 μm region as measured by Juno/JIRAM are dominated by the absorption bands of sulfur dioxide frost, which is ubiquitous at spatial scales of hundreds of km per pixel (e.g., Finale et al., 1979; Cruikshank et al., 1985; Carlson et al., 1997; Douté et al., 2001) and exhibits two strong signatures at ~4.07 μm and 4.37 μm, (entries #16 and #18 in table 2) respectively ascribed to the combination ν1+ν3 and the

149 overtone 2ν1 of SO_2, in addition to other six weaker features centered at approximately

150 2.92 μm (#7), 2.54 μm (#2), 2.79 μm (#5), 3.35 μm (#10), 3.56 μm (#12), and 3.78

151 (#13) (Nash and Betts, 1995; Nash and Betts, 1998).

152 Aside from SO_2 frost, JIRAM spectra reveal other features centered at about 3.9 μm

153 (3.85 and 3.91 μm, entries #14 and #15) and another pair of signatures centered

154 around 3.0 μm (2.97 and 3.16 μm, #8 and #9), which were previously observed both in

155 high-resolution infrared spectra obtained from Earth-based observations (Howell et al.,

156 1989) and in hyperspectral data acquired by Galileo NIMS (Carlson et al, 1997, 2007).

157 These features were interpreted to be due to the fundamental stretching modes in H_2S

158 and H_2O, respectively (Salama et al., 1990; Sandford et al., 1994), thus pointing to the

159 existence of H_2S/SO_2 and H_2O/SO_2 mixtures; Carlson et al., (1997, 2007) suggested that

160 a 3.15 μm feature could be oxyhydroxides (#9a). Indeed, pure H_2S could not survive as

161 it is extremely unstable at Io's surface, but Schmitt and Rodriguez (2003) derived an

162 upper limit of 0.01% for H_2S diluted in SO_2, while they alternatively suggest that Cl_2SO_2

163 with possible contribution by $ClSO_2$, diluted in solid SO_2, could be a good candidate for

164 the absorber(s) of the 3.92 μm band (#15b) locally present in NIMS spectra (Carlson et

165 al., 2007). Pure SO2 has a 3.93 μm band (#15c) which contributes to the band seen by

166 JIRAM (Schmitt and Rodriguez, 2003).

167 JIRAM spectra acquired at typical spatial resolutions of 100-150 km/px do not reveal

168 any signature at 2.85 μm diagnostic of sulfurous acid (H_2SO_3), which was suggested to

169 form through interaction of cryogenic SO_2 or SO_2/H_2O mixtures and high-energy photon

170 irradiation, and could survive at low temperatures (Voegele et al., 2004). Conversely,

171 absorption-like features show up at approximately 2.65 μm, 4.47 μm and 4.62 μm (#3,

172 #19 and #21). The 4.47-μm band could be ascribed to an overtone/combination of the

173 H_3O^+ molecule in sulfuric acid tetrahydrate, $H_2SO_4 \cdot 4H_2O$, which is a product of radiolysis

174 of SO_2 and H_2S in water ice (Moore et al., 2007). Baklouti et al. (2008) reported that the

175 $S^{16}O^{18}O$ isotope (2ν1 transition) is revealed by a diagnostic absorption feature at 4.48

176 μm, which indeed is observed in Galileo/NIMS data (#19b).

177 Among volatile compounds expected to be emitted by Io's volcanic vents and to

178 condense on the surface, CO_2 had been suggested (e.g., Sandford and Allamandola,

179 1993). However, the survival of condensed CO_2 depends on its residence time as a

180 function of temperature. In the 2-5 μm range, pure solid CO_2 and CO_2 intimately mixed

181   in a water ice matrix would produce a strong absorption band at 4.26 μm (#17a) and

182   weaker absorptions at 2.70 (#4) and 2.78 μm, whereas in JIRAM spectra we observe a

183   weak band at 4.26 μm (#17a), the 2.78 μm region is masked by the $2\nu1+\nu3$ combination

184   of SO_2, and at 2.70 μm there is only a hint of a potential inflection. On the other hand,

185   CO_2 in SO_2: H_2S ices also produces several additional bands. The 2.125 μm band, first

186   detected on Io by Trafton et al. (1991), was tentatively identified with CO_2 clusters in a

187   SO_2-dominated surface (Sandford et al., 1991). Therefore, the 2.1 μm and 4.26 μm-

188   features observed by JIRAM in principle could support the detection of CO_2 on Io.

189   However, the estimated positions for the $\nu1+\nu2$ combination and $2\nu2$ overtone bands of

190    $ClSO_2$ are ~4.28 μm and ~4.63 μm, which are close to the presumed CO_2 features, and in

191   addition to the 3.92-μm band make this molecule a highly interesting alternative or

192   competing candidate (Schmitt and Rodriguez, 2003). Also, Schmitt et al. (1994) later

193   interpreted the 2.123 μm feature as the SO2 $3\nu1+\nu1$ mode, so that the detection of CO_2

194   is only one potential explanation of the feature seen in JIRAM data.

195   Finally, we point out the presence of weak absorption bands, centered respectively at

196   3.4 μm and 4.55 μm (#11 and #20), which could be ascribed to the presence of organic

197   compounds and tholins, i.e. nitrogen-rich organics where the CN molecule is most likely

198   the spectrally active component. Among the Galilean satellites, such features were

199   already observed by NIMS on Callisto and Ganymede (McCord et al., 1997, 1998).

200   In Table 2 we summarize the spectral signatures visible in the average JIRAM spectra,

201   with relative assignment (either established or suggested) and bibliographic references.

202   During Juno's orbit 10 JIRAM collected images and spectra of Io, from a distance of

203   470,000 km (see table 1). The JIRAM FoV was tilted above and below the satellite to

204   allow the spectrometer slit to point to different locations on the surface. Hence, some of

205   the images only partially cover Io. In Fig. 3A we show a panel with selected spectral

206   radiance data and Fig. 3B we show the corresponding images from the same session.

207   In this section we begin the analysis of the spectrometer measurements with a

208   preliminary thermal characterization and, for this reason we consider only the

209   continuum where the wavelengths affected by SO_2 features have been excluded from

210   the data and replaced by a straight line (see figure caption for more details). Most of the

211   radiance spectra show either the intense solar reflected contribution (in the dayside) or

212   thermal emission at low temperature (in the night side). A retrieval of the temperature

213   map is not easily achievable from this dataset (see section 5). In fact, because of the

214   coarse spatial resolution (~100 km), which is much larger than many volcanic features

215   on Io (Veeder et al., 2012, 2015), the temperature is not uniform within a given JIRAM

216   pixel, and the thermal emission spectra are the result of the combination of thermal

217   emission coming from several sub-pixel hot features. Some selected spectra peak at

218   wavelengths between 3 and 4 μm, which indicates the presence of very hot structures

219   that do not fill completely the pixel FoV but whose emission is sufficiently intense to

220   distinguish them from the rest of the surface, which emits a lower-temperature Planck

221   distribution.

222   Some spectra, which we show in Fig. 3A, cannot be fitted with a single-temperature

223   Planck distribution. Also, single-pixel spectra may suffer of a small amount of spectral

224   tilt, i.e. when two different spectral regions of the same pixels "look" to slightly different

225   locations (Adriani et al., 2014; for JIRAM, spectral tilt has been calibrated and found no

226   larger than 0.01°; in-flight calibrations with Aldebaran – obtained on Jul. 20th 2016-

227   confirmed this value). Spectral tilt has the same magnitude as the pixel iFoV. Hence, in

228   the worst case, one pixel could have a hot, sub-pixel feature inside its FoV at 2 μm, and

229   outside its FoV at 5μm, causing the signal to drop at longer wavelengths. This could, in

230   principle, explain why some spectra are very sharp). Hence we start discussing them in

231   terms of peak wavelength.

232   Spectra *a, b* and *I* are from a location very close to Pele; *a* and *b* are also close to Pillan.

233   By using Wien's law (λ_{max} [μm] = 2898/T [K]) one can estimate that the effective

234   temperature of the observed feature is higher than 700 K, consistent with NIMS

235   observations of Pele (Davies et al., 2001). Spectrum *c* comes from an unidentified

236   feature close to Nemea (78°S, 320°W) and Aramazd Patera, and it is discussed as feature

237   #1 in Section 4. Spectra *d* and *e* are close each other and are tentatively assigned to

238   Sengen Patera. Spectrum *f* could be Ulgen Patera, spectrum *g* could be Viracocha Patera,

239   spectrum *h* could be Babbar Patera, spectrum *j* could be Pyerun. Features that could

240   produce the spectra *k, l m* and *n* are not firmly identified. In the case of hot spot *m*, the

241   peak wavelength is close to 2.5 μm, suggesting very high temperatures (~1100 K),

242   similar to some previously detected on Io (e.g. Spencer et al. 2007). In all cases, the

243   maximum radiance indicates that the areas at temperatures responsible for the peak

244   wavelength are extremely small with respect to the pixel, of the order of 1 square km,

245   hence can be ascribed to recent lava flows, lava flow break outs, lava fountains or lava

246   lakes (Lopes et al., 2004).

247   4. Super-resolution images

248   The images in the M band have been superimposed in order to increase the signal to

249   noise ratio and to apply a super-resolution algorithm. 20 images from orbit 10 have

250   been used to produce the result shown in Fig. 4 (left panel). The geometry of the

251   observation varies very little during this time (10 minutes, corresponding to a rotation

252   less than 1.5° in phase angle) so that, for simplicity, we assume the geometry of the

253   central image. Each image has been oversampled with cubic interpolation, then all

254   images have been aligned and merged. An *unsharp mask filter* has been applied to the

255   result to increase the resolution/contrast, without affecting the peak signal. The

256   reflected sunlight is not removed. In order to identify the observed features, a map of Io

257   features (Williams et al., 2011) has been projected onto a sphere and displayed in the

258   same vantage point configuration (Fig. 4, right).

259   The identification of the features in Fig. 4 is not always easy. Volcanoes on Io often

260   erupt lava flows that spread across the surface. Even at the resolution of the JIRAM

261   observations it is likely that the position of at least some thermal anomalies identified in

262   Voyager and Galileo data have changed, as was seen (for examples) at Prometheus

263   (McEwen et al., 1997) and Zamama (Davies and Ennis, 2011). Movement or

264   modification of the features is likely unless the hot spot is confined within a caldera, as

265   lava flows are likely to have moved and covered new areas since the last observations

266   from Galileo and Voyager(s). Here we focus on three features, indicated by arrows in

267   the figure.

268   Feature #1 (same as feature *c* in Fig 3A), at 80°S, 315°W could be the lava flows at

269   Nemea (East) (80.5°S, 320°W) or Nemea (West) (80.3°S, 330°W) (Veeder et al., 2009).

270   The Nemea region contained a hot spot detected by Voyager 1 IRIS in 1979 (Pearl and

271   Sinton, 1982), but not subsequently by Galileo or in ground-based observations (Lopes

272   et al., 2007). Alternatively, this thermal source could be Aramazd Patera (73.5°S,

273   338°W). Aramazd Patera has not previously been observed as a hot spot; it is a dark

274   patera, presumably silicate, and thus could be active now or recently reactivated.

275   Nemea Planum is a set of layered plains, although there are some dark flows at 80°S,

276   330°W that could be active (see Williams et al. map at pubs.usgs.gov/sim/3168/). The

277   peak radiance from Feature #1 is 30 mW m^{-2} sr^{-1} (spectral radiance is 60 mW m^{-2} μm^{-1}

278   sr^{-1}).

279   Feature #2, at *65°S, 240°W could possibly be Pyerun Patera (55.4°S, 251.1°W*; a dark

280   patera, it could have been reactivated) which was also a Voyager IRIS detection.

281   However, it is quite far from it (~ 300 km) and may be a previously undetected hot spot.

282   The peak radiance is 20 mW m^{-2} sr^{-1} (spectral radiance is 40 mW m^{-2} μm^{-1} sr^{-1}).

283   Feature #3, at 80°S, 180°W likely has not been previously detected. The nearest known

284   hot spot, the unnamed I32E detected by NIMS in orbits C20 and I32 (Lopes et al., 2007),

285   was located at 65.9S, 168.6 W. The large distance between I32E and our Feature #3

286   suggests it is unlikely that they are the same hotspot, and that this is a new hot spot

287   detection. The peak intensity is 3 mW m^{-2} sr^{-1} (spectral radiance is 6 mW m^{-2} μm^{-1} sr^{-1}).

288   Images from orbit 17 (taken on Dec. 21st 2018, with 70 km surface resolution) and orbit

289   18 (Feb., 12th 2019, same resolution) have also been processed in the same way. The

290   results are shown in Figure 5. In these images, the same hemisphere of Io is shown.

291   During orbit 17, JIRAM had the opportunity to see Io before and after entering the

292   eclipse behind Jupiter. Some of the most notable features have been identified and

293   marked with cyan text. Note that the data are very close to saturation, which is the

294   cause of the cross-shaped feature at 120W, 60N. By comparing the three images, it

295   appears that the majority of the hot spots are still active after two months, but a

296   considerable number of hot spots have varied in intensity (see caption of table 3 for

297   details). Hot spot number one in the table, for example, is a new detection and varied its

298   peak intensity from 11 to more than 40 mW sr^{-1} m^{-2} (because observation in orbit 18 is

299   saturated). In table 3, for some spots observed by JIRAM, the latitudes, longitudes, peak

300   intensity are listed (in the three cases: orbit 17 before eclipse, orbit 17 after eclipse,

301   orbit 18). The viewing geometries for orbit 17 and 18 are very close, but the solar zenith

302   angle is also given to take into account possible variations due to (mostly) illumination

303   and to surface temperature. None of the hot spots inside the yellow oval in Fig. 5 are

304   close to any entry in the comprehensive list of thermal sources produced by Veeder et

305   al. (2015) or Cantrall et al., (2018), so they are presumably observed by JIRAM for the

306 first time in Dec. 2018. Most of them are still visible two months later (Fig. 5, right
307 panel). These spots are marked with yellow color in table 3.

5. Spectral-derived temperatures

309 The solar radiation reflected from the surface is still detectable in the 4 to 5-µm spectral
310 range covered by JIRAM, as it can be seen from Figs. 3B, 4 and 5 obtained in the M-band
311 filter centered at 4.78 µm, where a separation between dayside and nightside is still
312 perceptible. In this case, a systematic thermal retrieval applied to the spectroscopic
313 dataset acquired by JIRAM can measure the natural thermal emission of Io with good
314 accuracy only in the hot spots, where surface temperatures can easily reach values as
315 high as hundreds of K at the spatial scale of JIRAM data (100-150 km/px in the first ten
316 orbits). On the rest of the dayside, the measured signal is essentially due to solar
317 reflection. As a result, surface temperature values obtained far away from the hot spots
318 are indeed to be interpreted as a thermal brightness associated to the measured
319 radiance.

320 Having made this necessary premise, here we describe the method used to retrieve
321 surface temperature from JIRAM spectral data, which we will also use in the future
322 when more spatially resolved data will be available. Such method is based on a Bayesian
323 approach to nonlinear inversion (Rodgers 2000) that already proved to be successful in
324 a number of cases: Rosetta/VIRTIS data of asteroid 21 Lutetia and comet
325 67P/Churyumov-Gerasimenko (Coradini et al. 2011; Keihm et al. 2012; Tosi et al.,
326 2019a), the entire set of infrared data acquired by the Dawn/VIR spectrometer at Vesta
327 and Ceres (Tosi et al. 2014, 2018, 2019b), and lunar data acquired by JIRAM itself
328 during the very first scientific observation taken at the Moon just before Juno's Earth
329 fly-by occurred on October 9, 2013 (Adriani et al., 2016). The basic assumptions of the
330 Bayesian algorithm here used are described in the Appendix of Tosi et al. (2014) as well
331 as in Section 4 of Adriani et al. (2016).

332 Unlike the Moon and the aforementioned minor bodies, the maximum daytime
333 temperature expected for the surface of Io within the thermal skin depth (of the order
334 of a few mm) is ~130 K (Rathbun et al., 2004). This value is well below the detection
335 threshold of JIRAM. This threshold is related to the instrumental in-flight noise (NESR,
336 defined in Section 2), which in turn is dominated by the spectrometer's temperature

11

and may vary over time from one Juno orbit to another. Within the first ten orbits, the JIRAM NESR was such that the minimum detectable temperature was typically around 170-180 K (in other words, this is the temperature that is retrieved for most sky background pixels). The radiance level due to the thermal emission measurable in the 4 to 5 μm range is two to four orders of magnitude lower than the NESR.

We applied the thermal retrieval separately on each pixel across the spectrometer's slit and in the 4.0-4.8 μm spectral range. Going through the geometric information derived for JIRAM spectroscopic data collected during a given Juno passage, one can ultimately obtain spatially resolved thermal maps of Io such as those shown in Fig. 6. The maximum temperatures, ∼250 K, are estimated with good accuracy and correspond to the major active volcanic centres.

From the literature it is known that Io's volcanic centers of Io erupt basaltic or ultramafic lavas at much higher temperatures, up to ∼1800 K for the Pillan hotspot from early Galileo analysis (McEwen et al., 1998; Davies et al., 2001), suggesting that lavas on Io are ultramafic, a type of lava that erupted mostly over a billion years ago on Earth and has a higher magma temperature than basaltic lavas. However, subsequent analysis of the same data by Kezthelyi et al. (2007) indicates a lower limit of ∼1600 K, consistent with basaltic to lunar-like compositions (such a temperature is consistent with some of the spectra in Fig. 3A, excluded from the database used for Fig. 6).

However, in the analysis presented in Fig. 6, the coarse spatial resolution of JIRAM data (in most cases between 100 and 150 km/px) implies that, for each JIRAM pixel, the recorded temperature is somewhat representative of the average temperature of the resolution cell. Because a pixel typically contains a range of lava temperatures, it is difficult to measure the hottest temperatures (typically corresponding to small areas) from remotely sensed data taken by JIRAM. We expect to improve these results when the spatial resolution of JIRAM spectral data will be ∼50 km or less (starting from 2020).

6. Summary and conclusions

The observation of the Galilean satellites by Juno is getting more feasible as the mission progresses, both because the Juno orbit is favourable, and because other concurrent, high-priority mission objectives have been achieved. For example, in orbit 25 (in early

2020), JIRAM is expected to have a very good chance to observe Io with a pixel resolution of ~50 km, and even better observations opportunities would occur if the mission is extended beyond 2021. In general, JIRAM will observe Io during about 50% of future orbits; every four months. This will result in a large database that, especially for the polar regions, would be unique and not achievable from Earth-based telescopic observations.

To prepare for the exploitation of future data, in this work we present preliminary results from Juno/JIRAM observations of Io. We presented average I/F spectra obtained in different orbits, which allow the identification of several spectral features on the surface. While SO_2 frost is ubiquitous at spatial scales of hundreds of km/px, and results in several absorption bands, JIRAM also detected additional absorptions potentially due to H_2O / SO_2 and H_2S / SO_2 mixtures; an interesting absorption feature at 4.47 μm, possibly hydronium in sulfuric acid tetrahydrate, or, alternatively, the $S^{16}O^{18}O$ isotope; another feature at 4.26 μm, which could be either CO_2 in SO_2 frost or $ClSO2$. JIRAM also detected some unidentified features not ascribable to known or expected instrumental artifacts, such as a clear absorption feature at 2.65 μm, which deserves further investigation.

Given the low temperatures typical of the surfaces of Galilean satellites, together with the spectral sensitivity range of JIRAM limited to 5 μm, a temperature retrieval can be attempted only for the hot spots, which are revealed both in the M-band imagery and in spectroscopic data acquired by JIRAM. There are several examples of JIRAM radiance spectra showing maxima in the spectral region between 2.5 and 4.0 μm. Assuming that the surface of Io behaves like a black body, according to Wien's law these maxima are indicative of local temperatures exceeding several hundred Kelvin. In some cases, temperatures are greater than 1000 K, similar to some of temperatures derived from Galileo NIMS data (Davies et al., 2001) from New Horizons data (Spencer et al., 2007; Rathbun et al. 2014) and from some ground based telescope observations (Marchis et al., 2002; de Pater et al., 2014; de Kleer et al., 2014). However, the measured radiance level is typically 10^4 to 10^6 times lower than the radiance provided by Planck's law, which - depending on the spatial resolution - is indicative of the size of the hottest sub-pixel features compared to the size of the JIRAM pixel. These are, presumably, the sum of the highest temperature areas of lava flows or lava lakes (few km^2).

Regions poorly covered before Juno, in particular the polar regions not covered by Voyager 1 observations, were imaged multiple times. Newly active hot spots have been identified in the South pole region, and many others at lower latitudes. In the future, the amount of data expected to be collected by JIRAM will enable a statistical study on the persistence and the distribution of hot spots; presently, it appears that most of the hot spots that JIRAM sees have a lifetime of at least a few months. Hot spots on Io tend to be long-lived, with many being active for years or even decades (Lopes-Gautier et al., 1999; Davies and Ennis, 2011; de Pater et al., 2017; Cantrall et al., 2018), though previous conclusions were largely based on data from the lower latitudes. The geometry of Juno's orbits and views of Io are therefore well suited to the investigation of possible differences in style of activity between the polar region hot spots and those at lower latitudes.

Mapping of the abundance of SO2 and of other chemical species revealed in JIRAM spectra will be the subject of future work. On the other hand, the strong absorptions of SO_2 frost make it difficult to retrieve the atmospheric column densities, because the wavelength position of gaseous SO_2 are quite close to the spectral counterparts of sulfuric surface compounds, and too weak to allow a safe retrieval. An atmospheric retrieval with limb data is not possible with this data set and could be attempted, in principle, only after JIRAM will acquire spectra from a much closer distance, enabling higher spatial resolution.

7. Data availability

Data in this study is publicly available on the Planetary Data System (http://pds.nasa.gov) and can be downloaded from http://atmos.nmsu.edu:8080/pds. The individual datasets are available at https://atmos.nmsu.edu/ PDS/data/jnojir_xxxx, where xxxx is 1001, 1002, or 1003 for EDR (Experiment Data Record; raw data) and 2001, 2002, or 2003 for RDR (Reduced Data Record; calibrated data) volumes.

8. Acknowledgments

9. References

433 Acton, C.H., (1996). Ancillary data services of NASA's navigation and ancillary
434   information facility. Planet. Space. Sci. 44 (1), 65-70

435 Adriani A, Coradini A, Filacchione G, Lonnie JI, Bini A, Pasqui C, Calamai L, Colosimo F,
436   Dinelli BM, Grassi D, Magni G, Moriconi ML, Orosei R. (2008). JIRAM, the image
437   spectrometer in the near infrared on board the Juno mission to Jupiter.
438   Astrobiology. 2008 Jun;8(3):613-22. doi: 10.1089/ast.2007.0167.

439 Adriani A., G. Filacchione, T. Di Iorio, D. Turrini, R. Noschese, A. Cicchetti, D. Grassi, A.
440   Mura, G. Sindoni, M. Zambelli, G. Piccioni, M.T. Capria, F. Tosi, R. Orosei, B.M. Dinelli,
441   M.L. Moriconi, E. Roncon, J.I. Lunine, H.N. Becker, A. Bini, A. Barbis, L. Calamai, C.
442   Pasqui, S. Nencioni, M. Rossi, M. Lastri, R. Formaro, A. Olivieri (2014), JIRAM, the
443   Jovian Infrared Auroral Mapper. Space Sci. Rev., DOI 10.1007/s11214-014-0094-y.

444 Adriani, A., Moriconi, M.L., Mura, A., Tosi, F., Sindoni, G., Noschese, R., Cicchetti, A.,
445   Filacchione, G., 2016. Juno's Earth flyby: the Jovian infrared Auroral Mapper
446   preliminary results. Astrophys. Space Sci. 361 (8), article id.272. Doi:
447   10.1007/s10509-016-2842-9.

448 Blaney, D. l., C. Hibbitts, R. O Green, R. N. Clark, J. B Dalton et al. (2019) The Europa
449   Clipper Mapping Imaging Spectrometer for Europa (MISE): Using Compositional
450   Mapping To Understand Europa. Lunar. Plan. Sci. Conf. 50, The Woodlands, TX,
451   Abstract number 2218.

452 Baklouti, D., Schmitt, B., Brissaud, O. (2008). S2O, polysulfuroxide and sulfur polymer on
453   Io's surface? Icarus. 194. 647-659. 10.1016/j.icarus.2007.11.016.

454 Bolton, S. J. , A. Adriani, V. Adumitroaie, M. Allison, J. Anderson, S. Atreya, J. Bloxham, S.
455   Brown, J. E. P. Connerney, E. Dejong, W. Folkner, D. Gautier, D. Grassi, S. Gulkis, T.
456   Guillot, C. Hansen, W. B. Hubbard, L. Iess, A. Ingersoll, M. Janssen, J. Jorgensen, Y.
457   Kaspi, S. M. Levin, C. Li, J. Lunine, Y. Miguel, A. Mura, G. Orton, T. Owen, M. Ravine, E.
458   Smith, P. Steffes, E. Stone, D. Stevenson, R. Thorne, J. Waite, D. Durante, R. W. Ebert,
459   T. K. Greathouse, V. Hue, M. Parisi, J. R. Szalay, R. Wilson, Jupiter's Interior And Deep

460   Atmosphere: The Initial Pole-To-Pole Passes With The Juno Spacecraft, Science26
461   May 2017 : 821-825.

462 Cantrall, C., K. de Kleer, I. de Pater, D. A. Williams, A. G. Davies. D. Nelson (2018)
463   Variability and geologic associations of volcanic activity on Io in 2001-2016, Icarus,
464   312, 267-294.

465 Carlson, R.W., Smythe, W.D., Lopes-Gautier, R.M.C., Davies, A.G., Kamp, L.W., Mosher, J.
466   A., Soderblom, L.A., Leader, F.E., Mehlman, R., Clark, R.N., Fanale, F.P., 1997.
467   Distribution of sulfur dioxide and other infrared absorbers on the surface of Io.
468   Geophys. Res. Lett. 24, 2479-2490. Doi: 10.1029/97GL02609.

469 Carlson, R.W., J.S. Kargel, S. Doute, L.A. Soderblom, and J.B. Dalton, 2007. Io's Surface
470   Composition. In: Lopes, R. and J.R. Spencer (Eds): *Io After Galileo*. Praxis Publishing
471   Company (Springer-Verlag, 2007).

472 Coradini, A. et al., 2011. The surface composition and temperature of Asteroid 21
473   Lutetia as observed by ROSETTA/VIRTIS. Science 334 (6055), 492-494. Doi:
474   10.1126/science.1204062.

475 Cruikshank, D.P., Howell, R.R., Fanale, F.P., Geballe, T.R., 1985. Sulfur dioxide ice on Io.
476   In: "Ices in the solar system"; Proceedings of the Advanced Research Workshop,
477   Nice, France, January 16-19, 1984 (A86-23051 09-91). Dordrecht, D. Reidel
478   Publishing Co., 1985, p. 805-815.

479 Davies, A. G., L. Wilson, D. L. Matson, G. Leone, L. Keszthelyi, W. Jaeger (2006) The
480   heartbeat of the volcano: The discovery of episodic activity at Prometheus on Io,
481   Icarus, 184, 460-477.

482 Davies, A. G. Volcanism on Io: A Comparison with Earth. Cambridge University Press,
483   Cambridge, UK. 372 pages, 2007.

484 Davies, A. G., L. P. Keszthelyi, D. Williams, C. Phillips, A. S. McEwen, R. Lopes, W.
485   Smythe, L. Kamp, L. Soderblom, R. Carlson. Thermal signature, eruption style and
486   eruption evolution at Pele and Pillan on Io. *Journal Geophys. Res*., 106, no. E12, 33,079-
487   33,104, 2001.

488 Davies, A. G., A.S. McEwen, R. Lopes-Gautier, L. Keszthelyi, R.W. Carlson and W.D.
489   Smythe Temperature and Area constraints of the South Volund volcano on Io from the

490   NIMS and SSI Instruments during the Galileo G1 orbit. Geophys. Res. Lettr., 24, 2447-
491   2450. doi: 0094-8534/97/97GL-0231050, 1997.

492   Davies, A. G., L. P. Keszthelyi and A. J. L. Harris. The Thermal Signature of Volcanic
493   Eruptions on Io and Earth, *JVGR,* 194, 75-99, doi:10.1016/j.jvolgeores.2010.04.009,
494   2010.

495   Davies, A. G. and M. E. Ennis. The variability of volcanic activity at Zamama, Culann, and
496   Tupan Patera on Io as seen by the *Galileo* Near Infrared Mapping Spectrometer,
497   *Icarus*, 215, 401-416, 2011.

498   Davies, A. G., G. J. Veeder, D. L. Matson and T. V. Johnson (2015) Map of Io's Volcanic
499   Heat Flow, Icarus, 262, 67-78. doi: http://dx.doi.org/10.1016/j.icarus.2015.08.003.
500   de Kleer, K., de Pater, I., Ádámkovics, M., Davies, A. G. (2014) Near-Infrared Monitoring of
501   Io & Detection of a Violent Outburst Gemini Eruption, *Icarus*, 242, 352-364. doi:
502   10.1016/j.icarus.2014.06.006.
503   de Kleer, K. & de Pater, I. Time Variability of Io's volcanic activity from near-IR adaptive
504   optics observations on 100 nights in 2013-2015. *Icarus*, 280, 378-404 (2016a).

505   de Kleer, K. and de Pater, I. Spatial distribution of Io's volcanic activity from near-IR
506   adaptive optics observations on 100 nights in 2013-2015. Icarus, 280, 405 (2016b).

507   de Pater, I., C. Laver, A. G. Davies, K. de Kleer, D. A. Williams, R. R. Howell, J. A. Rathbun
508   and J. R. Spencer (2016a) Io: Eruptions at Pillan, and the Time Evolution of Pele and
509   Pillan from 1996 – 2015, Icarus, 264, 198-212. doi 10.1016/j.icarus.2015.09.006.

510   de Pater, I., A. G. Davies and F. Marchis (2016b) Keck Observations of Eruptions on Io in
511   2003-2005. Icarus, 274, 284-296, doi: 10.1016/j.icarus.2015.12.054.

512   de Pater, I., K. de Kleer, A. G. Davies and M. Ádámkovics (2017) Three Decades of Loki
513   Patera Observations, *Icarus*, **297**, 265-281 doi: 10.1016/j.icarus.2017.03.016.

514   Douté, S., Lopes, R., Kamp, L.W., Carlson, R., Schmitt, B., 2004. Geology and activity
515   around volcanoes on Io from the analysis of NIMS spectral images. Icarus 169, 175-
516   196.

517   Douté, S., Lopes, R., Kamp, L.W., Carlson, R., Schmitt, B., and the Galileo NIMS Team,
518   2002. Dynamics and Evolution of SO2 Gas Condensation around Prometheus-like
519   Volcanic Plumes on Io as Seen by the Near Infrared Mapping Spectrometer. Icarus
520   158, 460-482.

521 Douté, S., Schmitt, B., Lopes, R., Carlson, R., Soderblom, L., Shirley, J., and the Galileo
522   NIMS Team, 2001. Mapping SO2 frost on Io by the modeling of NIMS hyperspectral
523   images. Icarus 149, 107-132. Doi: 10.1006/icar.2000.6513.

524 Fanale, F.P., Brown, R.H., Cruikshank, D.P., Clark, R.N., 1979. Significance of absorption
525   features in Io's IR reflectance spectrum. Nature 280, 761-763. Doi:
526   10.1038/280761a0.

527 Feaga, L. M. , M. McGrath, P. D. Feldman Io's dayside SO2 atmosphere, Icarus 201
528   (2009) 570–584, doi:10.1016/j.icarus.2009.01.029

529 Filacchione, G., Adriani, A., Mura, A., Tosi, F., Lunine, J. I., Raponi, A., Ciarniello, M., Grassi,
530   D., Piccioni, G., Moriconi, M. L., Altieri, F., Plainaki, C., Sindoni, G., Noschese, R.,
531   Cicchetti, A, Boltono, S. J., Brooks, S., 2019. Serendipitous infrared observations of
532   Europa by Juno/JIRAM, Icarus, 328, 1-13.

533 Hamilton, C.W., C.D. Beggan, S.Still, M.Beuthe, R.M.C. Lopes, D.A. Williams, W. Wright,
534   and J. Radebaugh (2013). Spatial Distribution of Volcanoes on Jupiter's Moon Io:
535   implications for tidal heating and magma ascent. Earth and Planetary Science
536   Letters, 361,272-286, doi.org/10.1016/j.epsl.2012.10.032

537 Howell, R.R., Nash, D.B., Geballe, T.R., Cruikshank, D.P., 1989. High-resolution infrared
538   spectroscopy of Io and possible surface materials. Icarus 78, 27-37. Doi:
539   10.1016/0019-1035(89)90067-5.

540 Keihm, S., Tosi, F., Kamp, L., Capaccioni, F., Gulkis, S., Grassi, D., Hofstadter, M.,
541   Filacchione, G., Lee, S., Giuppi, S., Janssen, M., Capria, M. Interpretation of combined
542   infrared, submillimeter, and millimeter thermal flux data obtained during the
543   Rosetta fly-by of Asteroid (21) Lutetia. Icarus 221 (1), 395-404. Doi:
544   10.1016/j.icarus.2012.08.002.

545 Keszthelyi, L., W. Jaeger, M. W., Milazzo, M., J. Radebaugh, J., A. G. Davies, K. L.A.G. and
546   Mitchell, K.L. (2007). New estimates for Io eruption temperatures: Implications for
547   the interior. *Icarus*, 192(2), pp.491-502.

548 Lopes, R.M., Spencer, J.R., 2007. Io after Galileo. ISBN 978-3-540-34681-4. Berlin:
549   Springer, 2007.

550   Lopes, R. and D. Williams (2005): Io after Galileo. *Reports on Progress in Physics*, Institute
551   of Physics Publishing, 68, 303-340.

552   Lopes, R., L. W. Kamp, W.D. Smythe, P. Mouginis-Mark, J. Kargel, J. Radebaugh, E.
553   P.Turtle, J. Perry, D.A. Williams, R.W. Carlson, S. Douté (2004). "Lava Lakes on Io.
554   Observations of Io's Volcanic Activity from Galileo during the 2001 Fly-bys. *Icarus*,
555   169/1, pp. 140-174.

556   Lopes-Gautier, R.; A.S. McEwen, W. Smythe, P. Geissler, L. Kamp, A.G. Davies, J. R.
557   Spencer, R. Carlson, F.E. Leader, R. Mehlman, L. Soderblom, and the Galileo NIMS and
558   SSI Teams. Hot Spots on Io: Global Distribution and Variations in Activity. *Icarus*,
559   vol.140, no. 2, pp. 243-264, 1999.

560   Marchis, F., D. Le Mignant, F. H. Chaffee, A. G. Davies, S. H. Kwok, R. Prangé, I. de Pater, P.
561   Amico, R. Campbell, T. Fusco *et al.* (2005) Keck AO survey of Io global volcanic
562   activity between 2 and 5 µm, *Icarus,* **176**, 96-122.

563   Marchis, F., I. dePater, A. G. Davies, H. G. Roe, T. Fusco, D. Le Mignant, P. Deschamps, B.
564   A. Mackintosh and R. Prange (2002) High-resolution Keck adaptive optics imaging of
565   violent activity on Io. Icarus, 160, 124-131.

566   Marchis et al., 2007 In: Lopes, R. and J.R. Spencer (Eds): *Io After Galileo*. Praxis Publishing
567   Company (Springer-Verlag, 2007).

568   Masursky, H., G.G. Schaber, L.A. Soderblom, R.G. Strom (1979). Preliminary geological
569   mapping of Io. Nature, 280, 725-729.

570   McCord, T.B., Carlson, R.W., Smythe, W.D., Hansen, G.B., Clark, R.N., Hibbitts, C.A., Fanale,
571   F.P., Granahan, J.C., Segura, M., Matson, D.L., Johnson, T.V., Martin, P.D., 1997.
572   Organics and other molecules in the surfaces of Callisto and Ganymede. Science 278,
573   271-275. Doi: 10.1126/science.278.5336.271.

574   McCord, T.B., Hansen, G.B., Clark, R.N., Martin, P.D., Hibbitts, C.A., Fanale, F.P., Granahan,
575   J.C., Segura, M., Matson, D.L., Johnson, T.V., Carlson, R.W., Smythe, W.D., Danielson,
576   G.E., and the NIMS team, 1998. Non-water ice constituents in the surface material of
577   the icy Galilean satellites from the Galileo near-infrared mapping spectrometer
578   investigation. J. Geophys. Res. 103 (E4), 8603-8626. Doi: 10.1029/98JE00788.

579 McEwen, A.S.; L. Keszthelyi, J.R. Spencer, G. Schubert, D.L. Matson, R. Lopes-Gautier, K.P.
580   Klaasen, T.V. Johnson, J.W. Head, P. Geissler, S. Fagents, A.G. Davies, M.H. Carr, H.H.
581   Breneman, M.J.S. Belton: Very High Temperature Volcanism on Jupiter's Moon Io.
582   Science, 281, 87-90, 1998.

583 McGrath, M.A., Belton, M.J.S., Spencer, J.R., Sartoretti, P., 2000. Spatially resolved
584   spectroscopy of Io's Pele Plume and SO2 atmosphere. Icarus 146, 476–493.

585 Moore, M.H., Hudson, R.L., Carlson, R.W., 2007. The radiolysis of SO2 and H2S in water
586   ice: Implications for the icy jovian satellites. Icarus 189, 409-423. Doi:
587   10.1016/j.icarus.2007.01.018.

588 Morabito, L.A., S.P. Synnot, P.N. Kupfermann, and S.A. Collins (1979). Discovery of
589   currently active extra-terrestrial volcanism. *Science* **204**, 972.

590 Nash D.B., and Betts B.H., 1995. Laboratory infrared spectra (2.3-23 µm) of SO2 phases:
591   Applications to Io surface analysis. Icarus 117 (2), 402-419. Doi:
592   10.1006/icar.1995.1165.

593 Nash D.B., and Betts B.H., 1998. Ices on Io – composition and texture. In: "Solar system
594   ices" (B. Schmitt, C. De Bergh, M. Festou, eds.). Kluwer, Dordrecht, pp. 607-638. Doi:
595   10.1007/978-94-011-5252-5_25.

596 Peale, S.J., P. Cassen, and R.T. Reynolds 1979. Melting of Io by tidal dissipation. *Science*
597   **203**, 892-894.

598 Perry, J., R. M. C. Lopes, J. R. Spencer, C. A. Alexander (2007). A summary of the Galileo
599   mission and its observations of Io. In: Lopes, R., and Spencer, J. R., eds. (2007). "Io
600   after Galileo." Praxis Publishing Company (Springer-Verlag), pp. 35-59.

601 Rathbun, J. A., Spencer, J. R., Tamppari, L. K., et al. 2004, Mapping of Io's thermal
602   radiation by the Galileo photopolarimeter–radiometer (PPR) instrument. Icarus,
603   169, 127-139.

604 Rathbun, J.; J.R. Spencer; R.M. Lopes; R.R. Howell (2014). "Io's Active Volcanoes During
605   the New Horizons Era: Insights from New Horizons Imaging". Icarus,
606   doi:10.1016/j.icarus.2013.12.002

607 Rathbun, J.A., Lopes, R.M.C., Spencer, J.R., The global distribution of active Ionian
608   volcanoes and implications for tidal heating models, AJ, 156, id.207, 2018.

609 Rodgers, C.D., 2000. Inverse Methods for Atmospheric Sounding: Theory and Practice.
610   World Scientific Publishing Co., Singapore.

611 Salama, F., Allamandola, L.J., Witteborn, F.C., Cruikshank, D.P., Sandford, S.A., Bregman,
612   J.D., 1990. The 2.5-5.0 micron spectra of Io - Evidence for H_2S and H_2O frozen in
613   SO_2. Icarus 83, 66-82. Doi: 10.1016/0019-1035(90)90006-U.

614 Sandford, S. A., Allamandola, L. J., 1990. The physical and infrared spectral properties of
615   CO_2 in astrophysical ice analogs. Astrophys. J. 355, 357-372. Doi: 10.1086/168770.

616 Sandford, S.A., Allamandola, L.J., 1993. The condensation and vaporization behavior of
617   ices containing SO_2, H_2S, and CO_2 - Implications for Io. Icarus 106, 478. Doi:
618   10.1006/icar.1993.1186.

619 Sandford, S.A., Geballe, T.R., Salama, F., Goorvitch, D., 1994. New narrow infrared
620   absorption features in the spectrum of Io between 3600 and 3100 CM (2.8-3.2
621   micrometers). Icarus 110 (2), 292-302. Doi: 10.1006/icar.1994.1123.

622 Sandford, S.A., Salama, F., Allamandola, L.J., Trafton, L.M., Lester, D.F., Ramseyer, T.F.,
623   1991. Laboratory studies of the newly discovered infrared band at 4705.2/cm
624   (2.1253 microns) in the spectrum of Io - The tentative identification of CO_2. Icarus
625   91, 125-144. Doi: 10.1016/0019-1035(91)90132-D.

626 Schmitt, B., and Rodriguez, S., 2003. Possible identification of local deposits of Cl_2SO_2
627   on Io from NIMS/Galileo spectra. J. Geophys. Res. 108 (E9), CiteID 5104. Doi:
628   10.1029/2002JE001988.

629 Smith, B.A., and the Voyager imaging team (1979). The Jupiter system through the eyes
630   of Voyager 1. *Science*, 204, 951-972.

631 Spencer, J.R. and N.M. Schneider 1996. Io on the eve of the Galileo mission. *Annu. Rev.*
632   *Earth Planet. Sci.* 24, 125-190.

633 Spencer, J.R., S.A. Stern, A.F. Cheng, H.A. Weaver, D.C. Reuter, K. Retherford, A. Lunsford, ,
634   J.M. Moore, O. Abramov, R.M.C. Lopes, J.E. Perry, L. Kamp, M. Showalter, K.L. Jessup,
635   F. Marchis, P.M. Schenk, C. Dumas (2007). Io Volcanism during the New Horizons
636   Jupiter Flyby: A Major Eruption of the Tvashtar Volcano. Science, 318, 240-243.

637 Spencer, J. R., K. L. Jessup, M. A. McGrath, et al. (2000). Discovery of gaseous S_2 in Io's

638   Pele plume. Science, 288, 1208–10.

639 Tosi, F., Capaccioni, F., M.T. Capria, F., et al., 2019a. The changing temperature of the

640   nucleus of comet 67P induced by morphological and seasonal effects. Nat. Astron.,

641   in press. Doi: 10.1038/s41550-019-0740-0.

642 Tosi, F., Capria, M.T., De Sanctis, M.C., et al., 2014. Thermal measurements of dark and

643   bright surface features on Vesta as derived from Dawn/VIR. Icarus 240, 36-57. Doi:

644   10.1016/j.icarus.2014.03.017.

645 Tosi, F., Carrozzo, F.G., Raponi, et al., 2018. Mineralogy and temperature of crater

646   Haulani on Ceres. Meteorit. Planet. Sci. 53 (9), 1902-1924. Doi:

647   10.1111/maps.13078.

648 Tosi, F., Carrozzo, F.G., Zambon, et al., 2019b. Mineralogical analysis of the Ac-H-6

649   Haulani quadrangle of the dwarf planet Ceres. Icarus 318, 170-187. Doi:

650   10.1016/j.icarus.2017.08.012.

651 Trafton, L.M., Lester, D.F., Ramseyer, T.F., Salama, F., Sandford, S.A., Allamandola, L. J.,

652   1991. Icarus 89, 264-276. Doi: 10.1016/0019-1035(91)90178-V.

653 Tsang, C., Rathbun, J., Spencer, J., Hesman, B., Abramov, O. (2014). Io's Hotspots in the

654   Near-Infrared Detected by LEISA During the New Horizons Flyby. Journal of

655   Geophysical Research: Planets. 119. 10.1002/2014JE004670.

656 Tyler, R. H., W. G. Henning and C. W. Hamilton, Tidal Heating in a Magma Ocean Within

657   Jupiter's moon Io. Astrophys. J. Suppl. Series, 218, 22, 17 pages, 2015.

658 Veeder, G. J., D .L. Matson, T. V. Johnson, D. L. Blaney, J. D. Goguen (1994). Io's heat flow

659   from infrared radiometry: 1983--1993. J. Geophys. Res. 99, 17095-17162.

660 Veeder, G. J., Davies, A. G., Matson, D. L., Johnson, T. V., Williams, D. A. and Radebaugh, J.

661   (2015) Io: Heat Flow from Small Volcanic Features, Icarus, 245, 379-410. doi:

662   10.1016/j.icarus.2014.07.028.

663 Veeder, G. J., A. G. Davies, D. L. Matson, T. V. Johnson, D. A. Williams and J. Radebaugh

664   (2012) Io: Volcanic Thermal Sources and Global Heat Flow, Icarus, 219, 701-722,

665   doi:10.1016/j.icarus.2012.04.004.

666 Veeder, G. J., A. G. Davies, D. L. Matson and T. V. Johnson (2009) Io: Heat flow from dark
667   volcanic fields, Icarus, 204, 239-253

668 Voegele, A.F., Loerting, T., Tautermann, C.S., Hallbrucker, A., Mayer, E., Liedl, K.R., 2004.
669   Sulfurous acid (H_2SO_3) on Io? Icarus 169 (1), 242-249. Doi:
670   10.1016/j.icarus.2003.11.012.

671 Williams, D.A., R. Greeley, R. Lopes-Gautier, A. G. Davies (2001): Evaluation of Sulfur
672   Flow Emplacement on Io from Galileo data and numerical modeling. Journal
673   Geophys. Res., vol. 106, no. E12, 33,161-33,174.

674 Williams, D.A., Keszthelyi, L.P., Crown, D.A., Yff, J.A., Jaeger, W.L., Schenk, P.M., Geissler,
675   P.E., and Becker, T.L., 2011, Geologic map of Io: U.S. Geological Survey Scientific
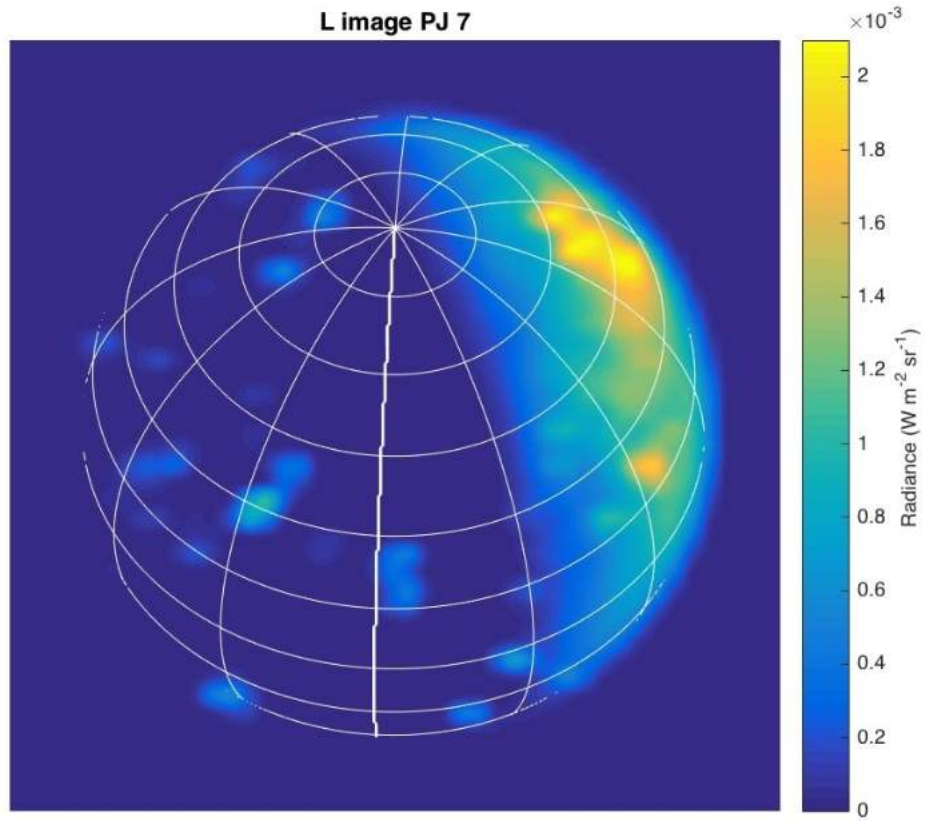676   Investigations Map 3168, scale 1:15,000,000, 25 p., available at
677   https://pubs.usgs.gov/sim/3168/.

678

L image PJ 7

679

680   ***Figure 1***. *L-band image of Io (radiance integrated from 3.3 to 3.6 μm), taken at UTC:2017-07-10 16:37:30,*

681   *during Juno's orbit 7. Meridians (30° apart) and parallels (15° apart) are superimposed (north hemisphere).*

682   *The thick meridian is 180° W. Sub-spacecraft point is 50°N, 176°W. Distance was 430'000 km. Similar images*

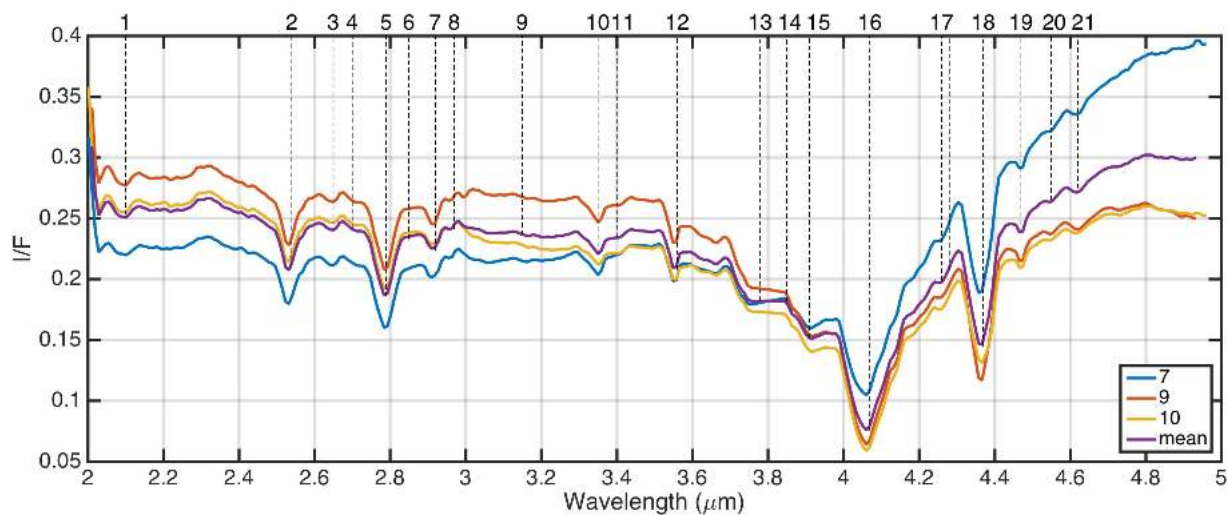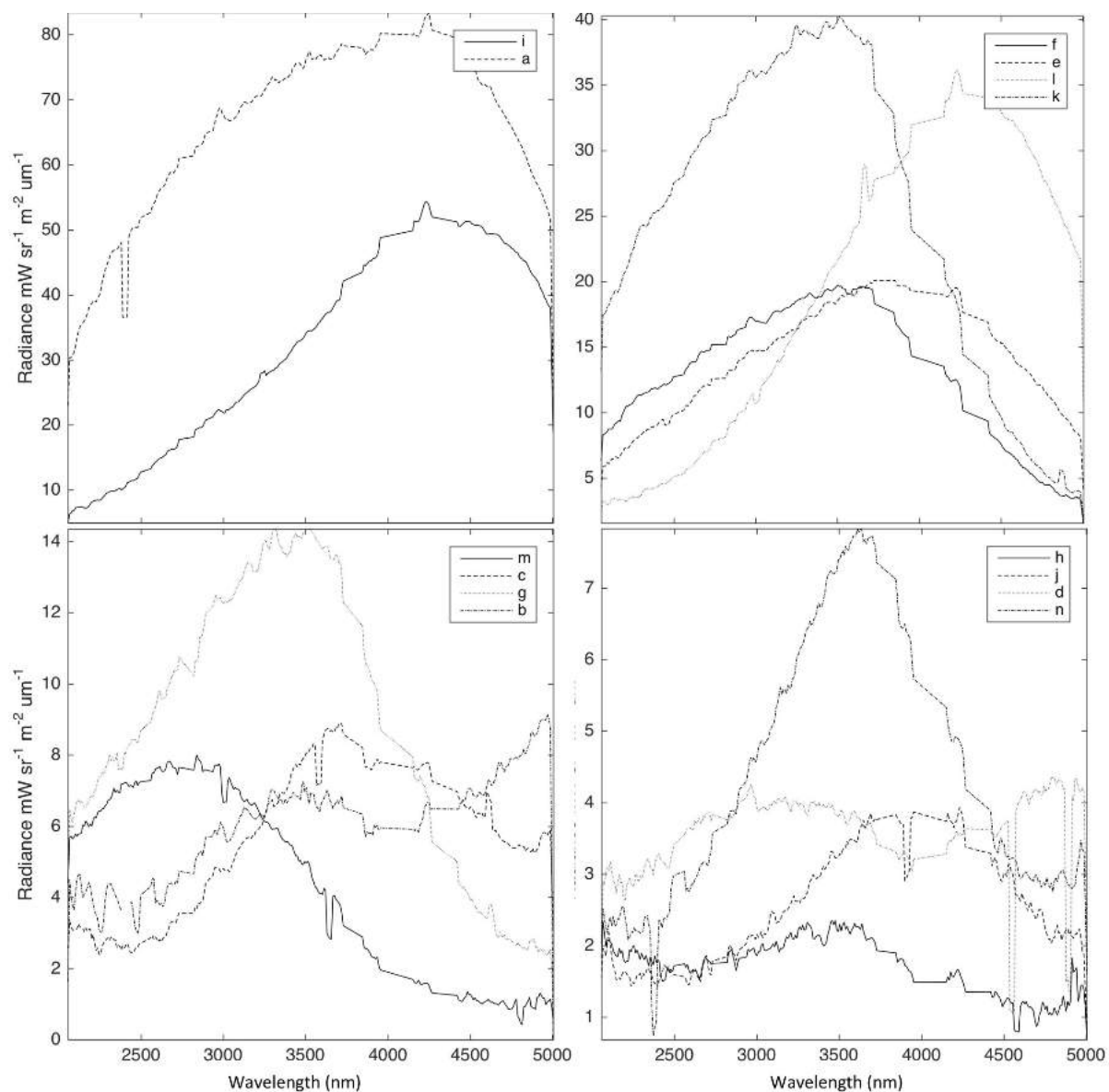683   *in band M are shown in Fig. 3B.*

684

685

Figure 2 *Dayside I/F computed from data from different orbits. Blue: orbit 7 (Jul. 10th 2017); Red: orbit 9;*
(Oct. 24th, 2017), Yellow: orbit 10 (Dec. 17th 2017); Magenta: average. Numbers on top refers to table 2, first
column.

690

691

692

Figure 3A: examples of spectra from Io's surface. The letters indicate the location on the surface, which is shown in figure 3B. JIRAM data from wavelengths affected by SO2 emission/absorption (*2002.3-2056.2 nm, 2514.7-2559.7 nm; 2748.5-2820.4 nm; 2910.3-2937.3 nm; 3746.5-3845.4 nm; 3971.3- 4151.1 nm; 4285.9-4420.8 nm*) have been removed from these spectra, and replaced with the continuum with a straight line.
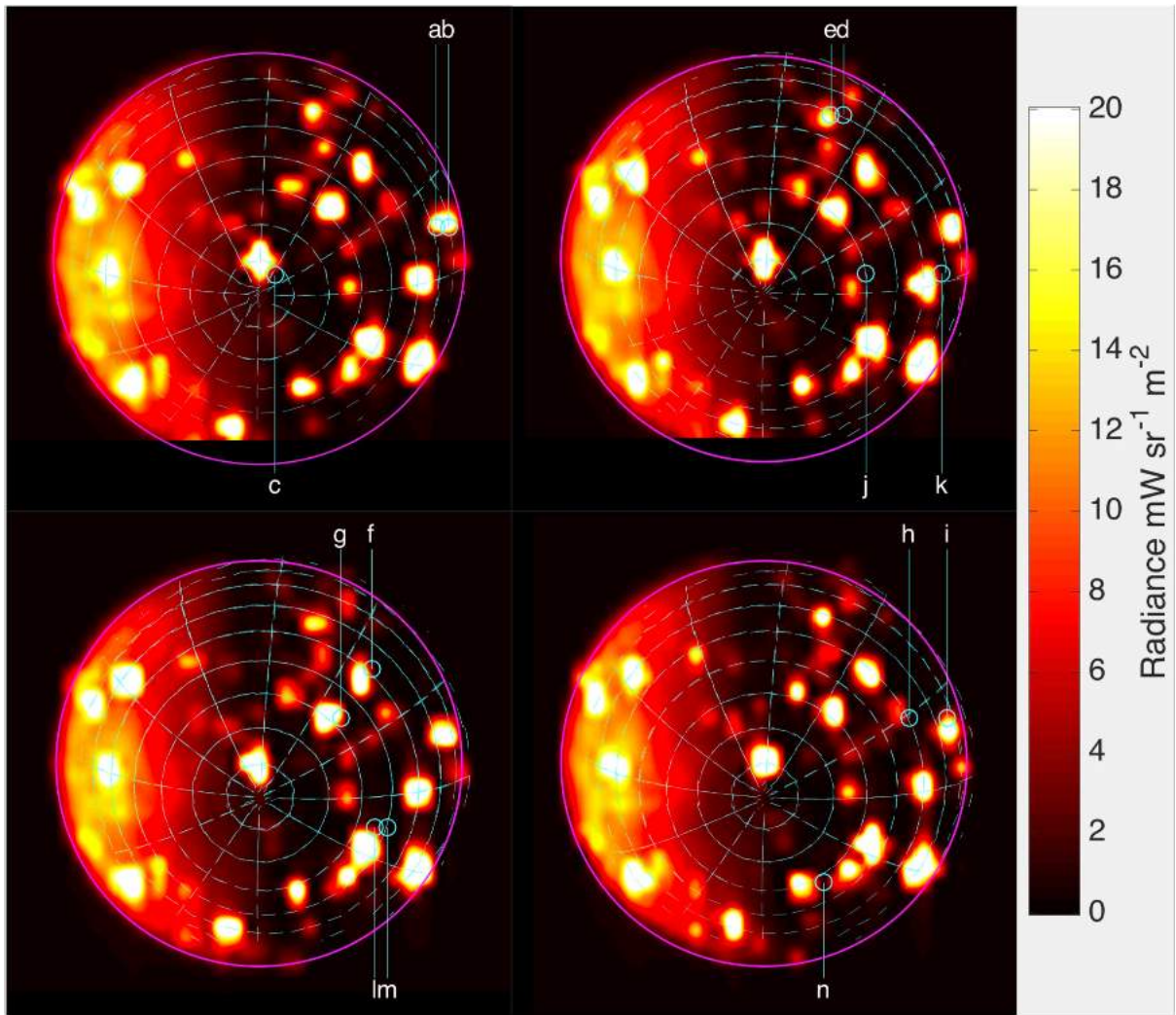
697

Figure 3B: examples of images of Io. The letters indicate the spectra in figure 2. Letters c, j, l, and n are relative to images that are simultaneous with the spectra, and are placed over the imager pixel that is co-aligned with the spectrometer pixel (the intrinsic error on spectrometer-imager alignment is of the order of one pixel). Other letters are placed in the correct position given by the SPICE reconstructed geometry (this implies an uncertainty of one or two pixels). The sub-solar spacecraft point is 319°W; 78°S. The pixel resolution is 110 km (same as the size of the circles indicating the positions).

706
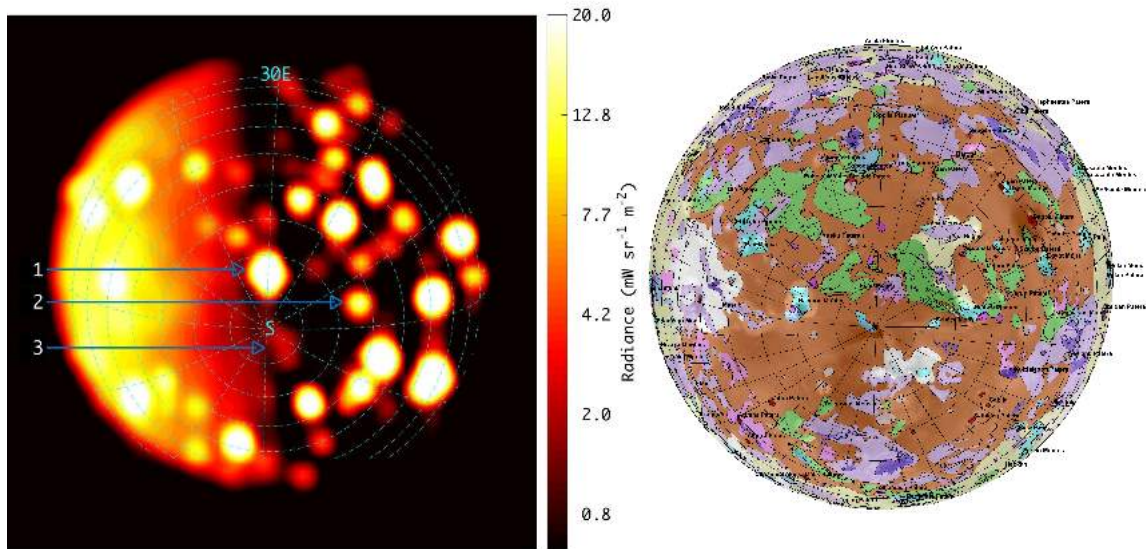
*Figure 4. Left. Infrared images in the M band taken during orbit 10 have been superimposed in order to increase the signal to noise ratio. Here we show the result, with meridians and parallels overlays. The 30° meridian is indicated, other meridians are every 30° and parallels are every 10°. **Right:** To identify the detected features, we show the Geologic map of Io (Williams et al. available at https://pubs.usgs.gov/sim/3168/), plotted in the same vantage point configuration as in the left panel. The parallel and meridians circles are the same as in the left panel. The sub-solar spacecraft point is 319°W; 78°S. The pixel resolution is 110 km.*

714

715
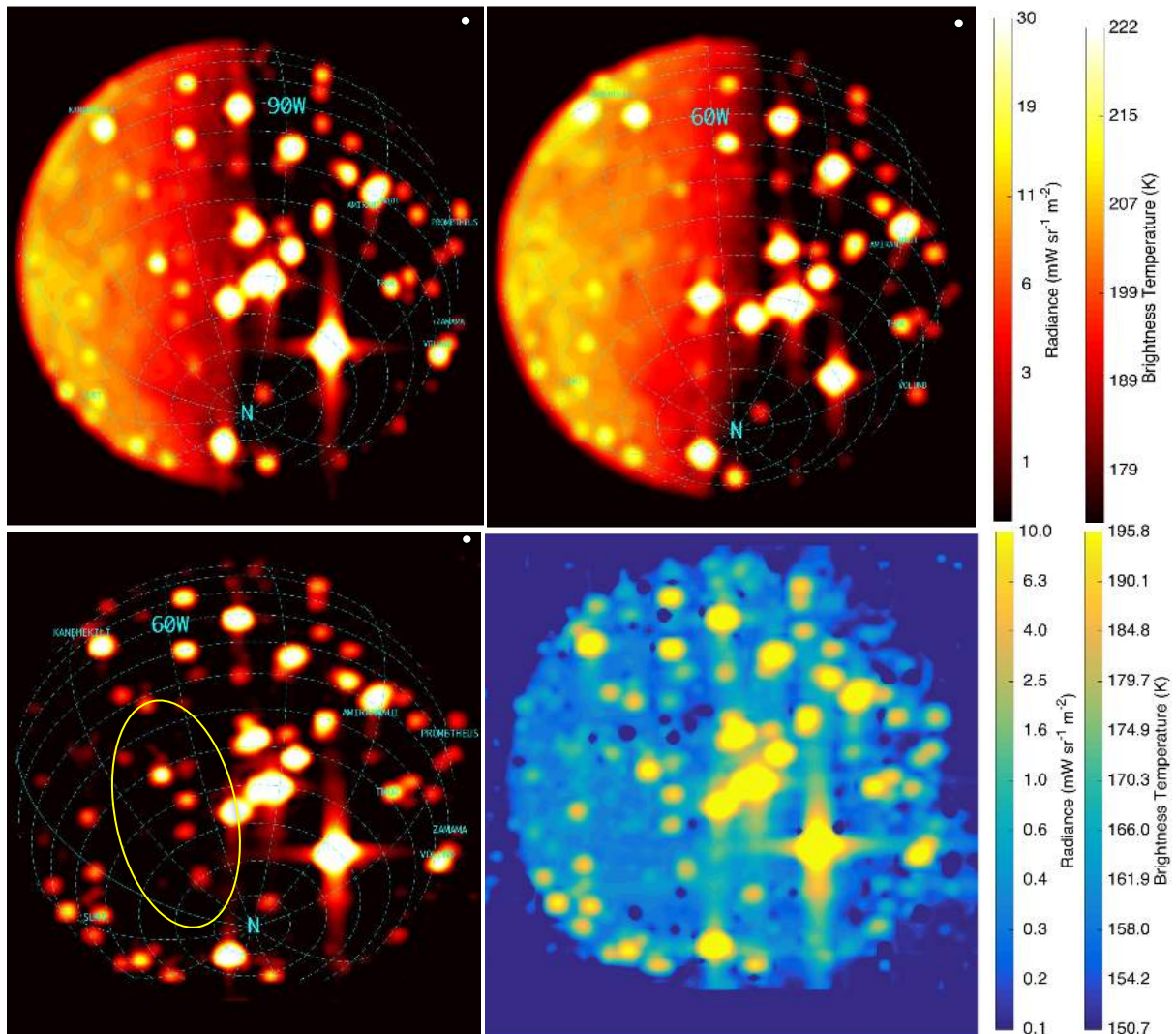
Figure 5. Top-left: Orbit 17 (Dec. 21st 2018), Io before eclipse (superimposition of 7 images). Bottom-left: orbit 17, Io during eclipse (2 images). Top-right: orbit 18 (Feb., 12th 2019, 14 images). Bottom-right: same, with colour scale stretched to show the faint thermal emission during eclipse. Sub-spacecraft point for orbit 17: 75°W, 48°N; for orbit 18: 60°W, 43°N. The surface resolution is 70 km, represented by the white circle on the top-right of each image (the size of the projected JIRAM pixel FoV). Brightness temperature is calculated assuming that the M band is 0.5 μm large and centred at 4.78 μm.
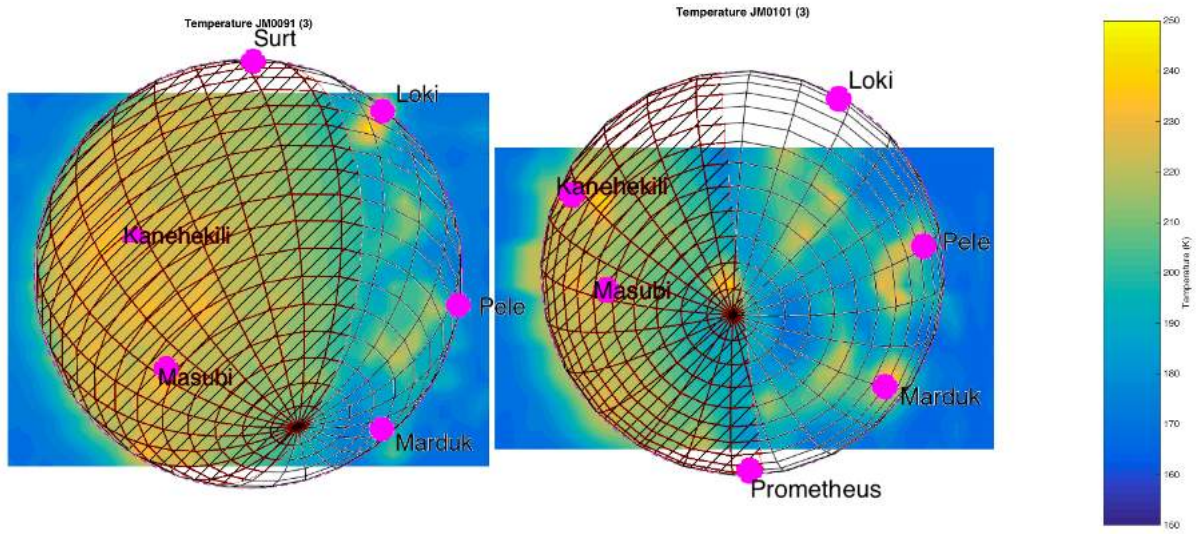
Figure 6. Spectral derived brightness temperature maps from orbits 9 and 10. Notable volcanos are indicated by magenta dots and labels. Spectra with sub-pixel structures have been excluded from the dataset. The spatial resolution is ~103 km/px and 113 km/px, respectively. Sub-spacecraft point for orbit 9: 4°W, 37°S; for orbit 10: 319°W, 78°S. Dayside is on the left, marked with a striped texture, to indicate the influence of the sunlight.

729

Table 1: list of observations of the M band and the spectrometer used for this study. Distance, Sub-Spacecraft Point (SSP) longitude and latitude refers to the center of the observation period

733

Orbit	Start UTC	Stop UTC	Number of observation	Distance (km)	SSP Longitude	SSP Latitude
7	2017-07-10 16:37:30	2017-07-10 17:12:48	59	420'000	183°W	52°N
9	2017-10-24 19:35:53	2017-10-24 20:16:46	71	430'000	4°W	37°S
10	2017-12-17 00:01:28	2017-12-17 00:19:52	34	470'000	319°W	78°S
17	2018-12-21 12:12:32	2018-12-21 12:35:17	43	300'000	75°W	48°N
18	2019-02-12 13:29:02	2019-02-12 13:47:35	38	300'000	60°W	43°N

734

736 **Table 2**: Spectral features identification. First column refers to figure 2.

#	Wavelenght (μm)	Assignment	Note	Reference
1	2.1	CO2 in SO2 frost		Trafton et al. (1991); Sandford et al. (1991)
2	2.54	SO2 overtone $3\nu_3$		Nash and Betts, (1995)
3	2.65	unidentified		
4	2.70	CO2 in SO2 frost	proposed	
5	2.79	SO2 combination $2\nu_1 + \nu_3$		Nash and Betts, (1995)
6	2.85	H2SO3	undetected	Voegele et al. (2004)
7	2.92	SO2 overtone $3\nu_1$		Nash and Betts, (1995)
8	2.97	H2O / SO2 mixture	suggested	Salama et al. (1990); Sandford et al., (1994)
9a	3.15	oxyhydroxides	suggested	Carlson et al. (1997)
9b	3.16	H2O / SO2 mixture	suggested	Salama et al. (1990); Sandford et al., (1994).
10	3.35	SO2 combination $\nu_1+\nu_2+\nu_3$		Nash and Betts, (1995)
11	3.4	Organics	proposed	
12	3.56	SO2 combination $2\nu_1+\nu_2$		Nash and Betts, (1995)
13	3.78	SO2 overtone $2\nu_3$		Nash and Betts, (1995)
14	3.85	H2S / SO2 mixture		Salama et al. (1990); Sandford et al., (1994)
15a	3.91	H2S / SO2 mixture	(*)	Salama et al. (1990); Sandford et al., (1994); Carlson et al. (2007)
15b	3.92	ClSO2 overtone 2ν1	alternative to (*)	Schmitt and Rodriguez (2003)
15c	3.93	Pure SO2	contributes to (*)	Schmitt and Rodriguez (2003)
16	4.07	SO2 combination $\nu_1 + \nu_3$		Nash and Betts, (1995)
17a	4.26	CO2 in SO2 frost	(**) proposed	Sandford and Allamandola (1990)
17b	4.28	ClSO2 combination $\nu_1+\nu_2$	alternative to (**)	Schmitt and Rodriguez (2003)
18	4.37	SO2 overtone $2\nu_1$		Nash and Betts, (1995)
19a	4.47	H_3O^+ overtone/combination in $H_2SO_4 \cdot 4H_2O$	(***)	Moore et al. (2007)
19b	4.47	$S^{16}O^{18}O$ isotope	alternative to (***)	Baklouti et al. (2008)
20	4.55	Tholins and nitriles	proposed	McCord et al. (1997); McCord et al. (1998)
21	4.62	ClSO2 overtone 2ν2		Schmitt and Rodriguez (2003)

737
738
739
Table 3: List of hot spots seen in figure 5. Hot spots from 1 to 12 have signal close to or above saturation (saturation radiance for these measurement is nominally 40 mW sr^{-1} m^{-2}; values above 30 should be handled cautiously and are indicated by grey background). Spectral radiances can be obtained by dividing by the bandpass value of 0.5 μm). Hot spots

1, 36, 36, 39, 40, 45 are those inside the yellow oval in figure 5 and are detected for the first time. Hot spots 37 and 38 are both close to a single one reported by Cantrall et al., (2018). Orbit 17 has two columns, one before eclipse (A) and one during eclipse (B). To help comparing cases 17A and 18, standard deviations of the peak signal are calculated. (*): very close to limb; (**): not detected. By comparing the data from orbit 17(A) and orbit 18, it appears that 9 out of 27 hot spots changed their intensity significantly (the difference of the two values is larger than the sum of the two standard deviations. If we consider only one standard deviation, then the number is 18 out of 27). Hot spots with radiance close to saturation (40 mW sr^{-1} m^{-2}) have been excluded from this count.

	Latitude (°)	Longitude (°W)	Peak signal (mW sr^{-1} m^{-2})			Solar zenith angle (°)	
			Orb. 17 (A)	Orb. 17 (B)	Orb. 18	Orb.17 (A)	Orb. 18
1	50.1±0.4	51.6±0.6	11.2±1.3	8.6	37.7±1.8	74	79.3
2	56.3±0.4	70.5±0.7	38.7±1.5	38.7	38±1.9	86.5	91.6
3	50.5±0.2	88.3±0.3	37.2±1.1	37.8	36.8±0.6	96.7	102.2
4	60.7±0.4	130.7±0.7	36.7±0.3	36.3	37.8±1.2	114	117.4
5	77.4±0.5	284.8±1	38.4±1.5	38	34.6±3.1	87.8	86.4
6	38.1±0.3	79.6±0.5	37.7±1.3	36.8	36.8±2.1	90.4	97.6
7	13.7±0.8	92±0.6	36.6±3	37.1	37.7±2	100.8	109.9
8	1.5±0.6	78.1±0.4	38.7±2.7	37	36.9±3	86.9	95.9
9	17.6±0.7	118.4±0.4	36.4±1.8	37	36.4±7.3	125.7	134.4
10	42.3±0.4	95.4±0.4	35.8±3	35.9	35±3.2	102.2	108.7
11	-3.9±0.6	40.7±0.3	36.4±1.6	36.8	36.2±2.2	49.6	58
12	-16.7±0	23.4±0	**	**	35.9±2.5	**	42.5
13	57.3±0.6	298.7±0.9	12.9±0.8	6.3	16.4±2.2	73.7	69.8
14	52.7±0.9	312.2±1.3	17.6±1.7	12.3	17.9±2.2	64.9	61.3
15	45.1±0.7	357.5±0.6	14.8±0.7	6.2	16.4±1	48.2	50
16	31±0.6	102.9±0.5	26.2±3.8	24.6	19.3±3.9	109.7	117.6
17	16.8±0.9	108.5±0.8	22.7±2.8	20.2	12.7±1.8	116.6	125.7
18	37.6±0.9	135.8±1.1	17.4±2.9	16	13.5±2.6	131.8	138.5
19	30.6±4	167.4±8.8	0.2±0.1	23.7	1.1±0.4	150.7	147.2
20	15±1.4	134.4±1.1	7.2±1.6	6.2	9.2±2.1	141	150.9
21	6.8±1.1	108.8±0.5	5.7±0.9	5.1	4.1±0.8	117.4	126.6
22	3.4±0.7	100.6±0.6	5.7±0.8	5.7	3.5±0.6	109.1	118.5
23	-9.4±1.3	100.8±0.7	5.4±1.3	3.8	3.5±0.9	108.4	117.4
24	-20.6±1.6	103.6±1.4	8.5±1.5	6.8	6.5±1.6	109	118.3
25	20.1±0.6	77.3±0.4	4.8±0.5	4.1	4.4±0.6	87.3	95.7
26	10±0.4	63.6±0.3	27.5±2.5	25.9	27.5±3.8	73.2	81.9
27	-10.8±0.9	64.8±0.3	21.4±3.1	17.8	12±1.5	73.5	81.9
28	81.6±0.5	109.1±0.4	4±0.8	2.7	3.4±0.8	96.5	98
29	36.2±0.6	91.2±0.6	6.7±1.4	7.2	5.9±1	99.6	107.1
30	26±1.3	152.4±1.5	4.4±0.9	4	2.6±0.6	149.8	156.4
31	15.9±1.7	150.1±0.4	3.5±0.8	3.1	1.3±0.3	154	162.7
32	34.4±0.7	121.4±0.3	2.1±0.2	2.1	1.4±0.4	123.6	130.6
33	67.3±0.8	243±1.3	13±1.8	8.9	14.3±2.7	99	96.6
34	69.4±0.7	36.2±2.2	7±0.7	3.2	**	78.7	**
35	57.3±0	44.3±0.8	7±0.5	3.7	**	73.9	**
36	41.7±0	46.5±0.2	25.3±3.2	25.2	**	67.4	**
37	22±0.6	49.8±0.2	10.4±2	5.8	10.5±1	62.9	70.1
38	16.7±0.1	43.7±0.1	11.7±2.1	4.5	9.8±0.3	56	63.6
39	32.8±0	37.6±0	**	2.2	**	**	**
40	36.8±0.3	14.5±0.8	14.3±0.5	5.4	15.9±0.9	45.1	50.1
41	47.7±0.3	338.2±0.8	17±1.3	8.9	16.2±1.1	52.2	50.9
42	41.2±0.7	324.1±0.7	12.5±0.8	4.7	13.8±0.9	51.2	47.3
43	32.8±1.2	330.1±0.8	15.9±2.3	10.9	14.9±1.6	41.3	37.2
44	29.9±1	339.1±0.4	**	3.5	11.8±0.9	**	32.6
45	42.7±0	56.1±0	**	2.1	**	**	**
46	18.2±0.7	65.9±0.2	**	2	3.9±0.2	**	84.7
47	37.6±0	199.2±0	**	2.1	**	**	**
48	2.5±0	149.6±0	**	0.6	**	**	**